Topics in Catalysis (2018) 61:1257–1262
https://doi.org/10.1007/s11244-018-0980-8

ORIGINAL PAPER

Surface Spectroscopic Analysis of TiO_2 and ZnO Nanoparticles Doped with Noble Metals

Hangil Lee[1] · **Jung A. Hong**[1]

Published online: 3 May 2018

Abstract

Nanoparticles (NPs) of the well-known photocatalysts TiO_2 and ZnO each doped with noble metals (NM = Au, Pd, or Pt) were synthesized by applying a thermosynthetic method, and the catalytic activities of the resulting six samples were compared. After characterizing them by using high-resolution photoemission spectroscopy (HRPES), we evaluated the catalytic effects of the samples the oxidation of 4-aminothiophenol (4-ATP) by using HRPES under UV illumination and on the oxidation of 4-ATP in aqueous solution by taking electrochemistry measurements. In addition, we determined the rates of conversion of CO to CO_2 in the presence of these catalysts by using a residual gas analyzer under an ultra-high vacuum condition. As a result, we found a good positive correlation between the numbers of defect structures induced by the doped noble metals and the catalytic activity, and showed that Pd-TiO_2 and Pt-ZnO NPs can act as efficient catalysts due to their relatively large number of defect structures and corresponding oxygen vacancies.

Graphical Abstract

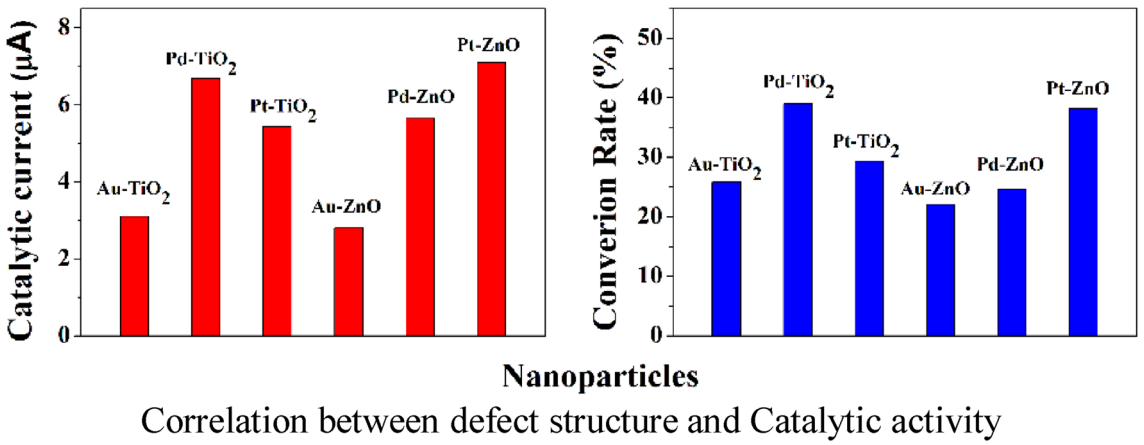

Keywords Noble-metal-doped metal oxide · Catalyst · Defect structure · Photocatalytic oxidation · HRPES · Electrochemistry

1 Introduction

The metal oxides TiO_2 and ZnO have been known for several decades to display effective catalytic activities and to be stable and inexpensive; they have therefore garnered significant attention and have been used in various applications such as solar cells, photocatalysis, and electrochemical

✉ Hangil Lee
easyscan@sookmyung.ac.kr

[1] Department of Chemistry, Sookmyung Women's University, Seoul 140-742, Republic of Korea

catalysis [1–6]. However, they have relatively wide band gaps ($E_g = 3.0 \sim 3.4$ eV) and hence absorb only UV light [7–12]. Therefore, significant efforts have been applied toward narrowing their band gaps and further enhancing their catalytic activities, with these efforts including the doping of other elements [13]. Various dopants such as metals or anions have been studied in this regard, and noble metals in particular have, as dopants or co-catalysts, been shown to be very effective at enhancing the photocatalytic activities of TiO_2 and ZnO nanoparticles (NPs) but with the drawback of being expensive. Metal oxides doped with noble metals are nevertheless very good for systematic model studies of catalytic reactions because they themselves can act as good catalysts [14–17]. Hence, comparing the catalytic activities among them, it is easy and clear to confirm the changes of catalytic reactions depending on outside efforts (noble metal doping).

For these purposes, we inserted noble metals (Au, Pd, or Pt) as dopants into TiO_2 and ZnO NPs and found the doping to significantly enhance their catalytic performances. We successfully fabricated the corresponding six noble-metal-doped metal oxide (NM-MO) NPs, i.e., Au-TiO_2, Pd-TiO_2, Pt-TiO_2, Au-ZnO, Pd-ZnO, and Pt-ZnO, using a thermosynthetic process (see Sect. 2). We first compared their electronic properties by using high-resolution photoemission spectroscopy (HRPES). And then we assessed their catalytic capacities by using them to oxidize 4-aminothiophenol (4-ATP) under ultra-high vacuum (UHV) conditions with 365-nm-wavelength UV light illumination by using HRPES and monitoring the resulting changes in their cyclic voltammograms (CVs) in the solution phase, as well as by using them to catalyze the conversion of CO to CO_2 and monitoring this conversion using mass spectroscopy. Through the spectral analyses, we found the catalytic properties of the Pd-TiO_2 and Pt-ZnO NPs to be better than those of the Au-TiO_2, Pd-TiO_2, Au-ZnO, or Pd-ZnO NPs. We attributed this difference to PdO (or PtO) formed on the NP surfaces making more defect structures on the TiO_2 or ZnO NPs and then increasing the rate of the photocatalytic reactions.

2 Experimental

2.1 Preparation of Precursor Solutions

We prepared each precursor solution by using a one-pot synthesis. The desired amounts of the noble metal (NM) dopants were added in the form $PtCl_2$ (99%), $PdCl_2$ (98%), $AuCl_3$ (98%) and expressed as mole fractions with respect to TiO_2 or ZnO [NM/(NM + TiO_2) or NM/(NM + ZnO)]. All substances were purchased from Sigma-Aldrich. The precursor solutions were stirred for ten minutes. 4-Aminothiophenol (4-ATP, Sigma-Aldrich, 97%), and Nafion (Sigma-Aldrich, 5 wt% in a low-molecular-weight aliphatic alcohol and water) were purchased from Sigma-Aldrich. Phosphate-buffered saline (PBS) tablets were purchased from Gibco.

2.2 Preparation of Noble-Metal-Doped TiO_2 or ZnO NPs

Tetramethylammonium hydroxide (TMAOH) (1.2 g) was diluted with double-distilled water (DDW, 22.25 g). Titanium isopropoxide (TTIP, 3.52 g) was diluted with isopropanol (3.5 g). Both of these solutions were stirred separately for 10 min. The TTIP solution was added dropwise to the TMAOH solution at room temperature, and this addition resulted in the appearance of white TiO_2. A solution of 10 mM $Zn(CH_3COO)_2{\cdot}2H_2O$ (Junsei, 99%) in 1-propanol (Sigma-Aldrich, 99.7%) was heated on an oil bath at 100 °C for 10 min. And then, this seed solution containing 25 mM $Zn(NO_3){\cdot}6H_2O$ (Junsei, 96%), 25 mM hexamethylenetetramine (Sigma-Aldrich, 99%), and 4 g/L polyethyleneimine (Sigma-Aldrich, branched, $M_W \sim 25{,}000$) was placed in a Teflon-lined autoclave in an oven at 180 °C for 7 h to perform the hydrothermal syntheses. And then, the desired amounts (3 wt%) of the noble metal dopants ($PtCl_2$, $PdCl_2$, $AuCl_3$) were added to each synthetic gel solution in an oil bath at 80 °C with stirring. After approximately 10 min, the synthetic gel solution became transparent. The solutions were transferred to Teflon-lined autoclaves and then sealed and heated at 220 °C for 7 h in a convection oven. The resulting NM-TiO_2 and NM-ZnO (Au-TiO_2, Pd-TiO_2, Pt-TiO_2, Au-ZnO, Pd-ZnO, and Pt-ZnO) were filtered and washed with DDW to remove any residue.

2.3 Oxidation Reactions

4-Aminothiophenol (4-ATP, Sigma-Aldrich, 99.9%) was purified using turbo pumping to remove impurities. Then, a direct dozer controlled by means of a variable leak valve was used to dose the purified 4-ATP onto the NM-TiO_2 or NM-ZnO NPs. The pressure of the chamber was 10^{-6} torr during the dosing. Various amounts of 4-ATP, between $0 \sim 180$ Langmuir (L), were made to be exposed to the six samples by applying various dosing times from $0 \sim 180$ s. We irradiated the system containing 4-ATP and molecular oxygen with UV light ($\lambda = 365$ nm, VL-4. LC Tube 1 × 4-Watt, Vilber Loumat) to increase the rates of the catalytic reactions.

2.4 Fabrication of NM-TiO_2 and NM-ZnO-Nafion-Modified GCEs and Electrochemical Measurements of 4-ATP Oxidation

The electrochemical oxidation of 4-ATP was investigated using glassy carbon electrodes (GCEs) modified with

NM-TiO_2 or NM-ZnO NPs. For each NM, a mass of 4.0 mg of NM-TiO_2 or NM-ZnO was dispersed into 1.0 ml of distilled water containing 50 µl Nafion, and then mixed by using an ultrasonic processor for 10 min to obtain a homogeneous NM-TiO_2 or NM-ZnO-Nafion mixture. Then, a volume of 20 µl of the mixture was placed on a GCE, and was dried at 75 °C in a pre-heated oven for 30 min. A cyclic voltammogram (CV) of 10 mM 4-ATP in PBS was obtained for each NM-TiO_2- or NM-ZnO-Nafion-modified GCE.

2.5 Characterization

High-resolution photoemission spectroscopy (HRPES) experiments were performed at the 8A1 beamline of the Pohang Accelerator Laboratory (PAL), which was equipped with an electron analyzer (PHI-3057). The electrochemical experiments were performed by using a CHI620E potentiostat (CH Instruments, Austin, TX) with a three-electrode cell placed in a Faraday cage. A GCE with a diameter of 2 mm was used as the working electrode, a Pt wire with a diameter of 1 mm was used as the counter electrode, and the reference electrode was Hg/HgO (1 M KOH). In addition, the rate of the oxidative conversion of CO to CO_2 was acquired by using a Hiden RC 301 mass spectrometer (mass range ~ 300 amu).

3 Results and Discussion

Core-level spectra of the Au-TiO_2, Pd-TiO_2, and Pt-TiO_2 NPs (Fig. 1a, from top to bottom) were acquired to determine their electronic properties, which would be expected to be closely correlated with their catalytic activities. All three noble metal (NM)-TiO_2 NPs yielded two distinctive sets of HRPES features: Ti $2p_{3/2}$ features at 459.3 eV (Ti^{4+}) and 457.9 eV (Ti^{3+}) and O 1*s* features at 530.5 eV (O1; TiO_2) and ~ 529.5 eV (O2; Au^{3+}-, Pd^{2+}-, and Pt^{2+}-induced peaks) due to the doped metals (Au, Pd, and Pt). Additionally, these doped noble metals also yielded two distinct peaks each: Au $4f_{7/2}$ peaks at 84.0 eV (Au^0) and 87.9 eV (Au^{3+}), Pd $3d_{5/2}$ peaks at 335.7 eV (Pt^0) and 336.5 eV (Pd^{2+}), and Pt $4f_{7/2}$ peaks at 72.6 eV (Pt^0) and 73.8 eV (Pt^{2+}) [18–24]. TiO_2 (Ti^{3+}) defect structures were previously reported to be closely related to catalytic activity [25, 26]. Hence, based on the observed intensity of the Ti^{3+} peak of the Pd-TiO_2 NPs being greater than those of the Au- or Pt-TiO_2 NPs, and also based on the intensity of its O_2 (PdO peak) being greater as well (see the middle panel of Fig. 1a), we predicted the catalytic activity of the Pd-TiO_2 NPs to be greater than those of other two NM-TiO_2 NPs. In other word, the Ti^{3+} defect structure has also been shown, because of charge compensation, to be related to oxygen vacancy states in TiO_2 as these removed oxygen atoms from TiO_2 have been suggested to be used to form PdO [27].

Core-level spectra of the NM-ZnO NPs were also acquired (Fig. 1b, from top to bottom). Each of the three NM-ZnO NPs also yielded two distinctive sets of features: Zn $3p_{3/2}$ features at 90.1 eV (Zn^{2+}) and 89.4 eV (Zn^{+}) and O 1*s* features at 531.9 eV (O3; ZnO) and 529.5 eV (O4; Au^{3+}-, Pd^{2+}-, and Pt^{2+}-induced peaks) due to the doped metals (Au, Pd, and Pt) [28, 29]. Additionally, these doped noble metals also yielded two distinct peaks; Au $4f_{7/2}$ at 84.0 eV (Au^0) and 85.4 eV (Au^{3+}), Pd $3d_{5/2}$ at 335.7 eV (Pd^0) and 336.5 eV (Pd^{2+}), and Pt $4f_{7/2}$ at 72.6 eV (Pt^0) and 73.8 eV (Pt^{2+}) [18–24]. In particular, the O 1*s* peak at 531.9 eV (O_3) indicated the presence of oxygen defects in the ZnO NPs. Hence, we also expected the catalytic activity of the Pt-ZnO NPs to be greater than the activities of the Au-ZnO and Pd-ZnO NPs, as the intensity of the oxygen defect peak resulting from the Pt-ZnO NPs was markedly higher than those of the Au-ZnO and Pd-ZnO NPs, as shown in Fig. 1b. In order to compare the amounts of defect structures in the six samples, the ratios of the intensities of the main and defect structure Ti and Zn peaks were calculated. These ratios for Au-TiO_2, Pd-TiO_2, Pt-TiO_2, Au-ZnO, Pd-ZnO and Pt-ZnO were calculated to be 0.098, 0.207, 0.140, 0.149, 0.239 and 0.407, respectively. That is, Pd-TiO_2 and Pt-ZnO showed the most defect structures. Based on these results, we took electrochemistry (EC) measurements and performed photocatalytic reactions for the six different samples to compare their catalytic activities.

CVs were obtained from a PBS solution containing 10 mM 4-ATP at a bare GCEs and those modified with the NM-TiO_2 or ZnO-Nafion catalysts, with each system irradiated with 365 nm wavelength UV light (Fig. 2). A sluggish oxidation current of 1.8 µA was observed at the bare GCE. This sluggishness was due to the intrinsically slow oxidation of 4-ATP (not shown here). In contrast, the currents associated with the oxidation of 4-ATP were 6.7 (±0.5) and 7.1 (±0.6) µA when using the GCEs modified with the Pd-TiO_2 and Pt-ZnO NPs, respectively (not shown here), significantly greater (i.e., 3.72 and 3.94 times greater) than that for the bare GCE. The currents generated when using the Au-TiO_2, Pt-TiO_2, Au-ZnO, and Pd-ZnO NPs, however, were only 3.1 (±0.3), 5.4 (±0.4), 2.8 (±0.3), and 5.7 (±0.4) µA, respectively (not shown here), which were slightly (1.72, 3.00, 1.55, and 3.17 times) but not significantly greater than that for the bare electrode. These results revealed the importance of the type of noble metal doped into the TiO_2 and ZnO NPs for catalyzing oxidation reactions, even when using 3 wt% of the doped noble metals, and specifically indicated the Pd-TiO_2 and Pt-ZnO NPs to be good catalysts for the oxidation of 4-ATP. Further investigations involving the optimization of the conditions are needed in order to selectively and sensitively detect 4-ATP using Pd-TiO_2 and Pt-ZnO NPs.

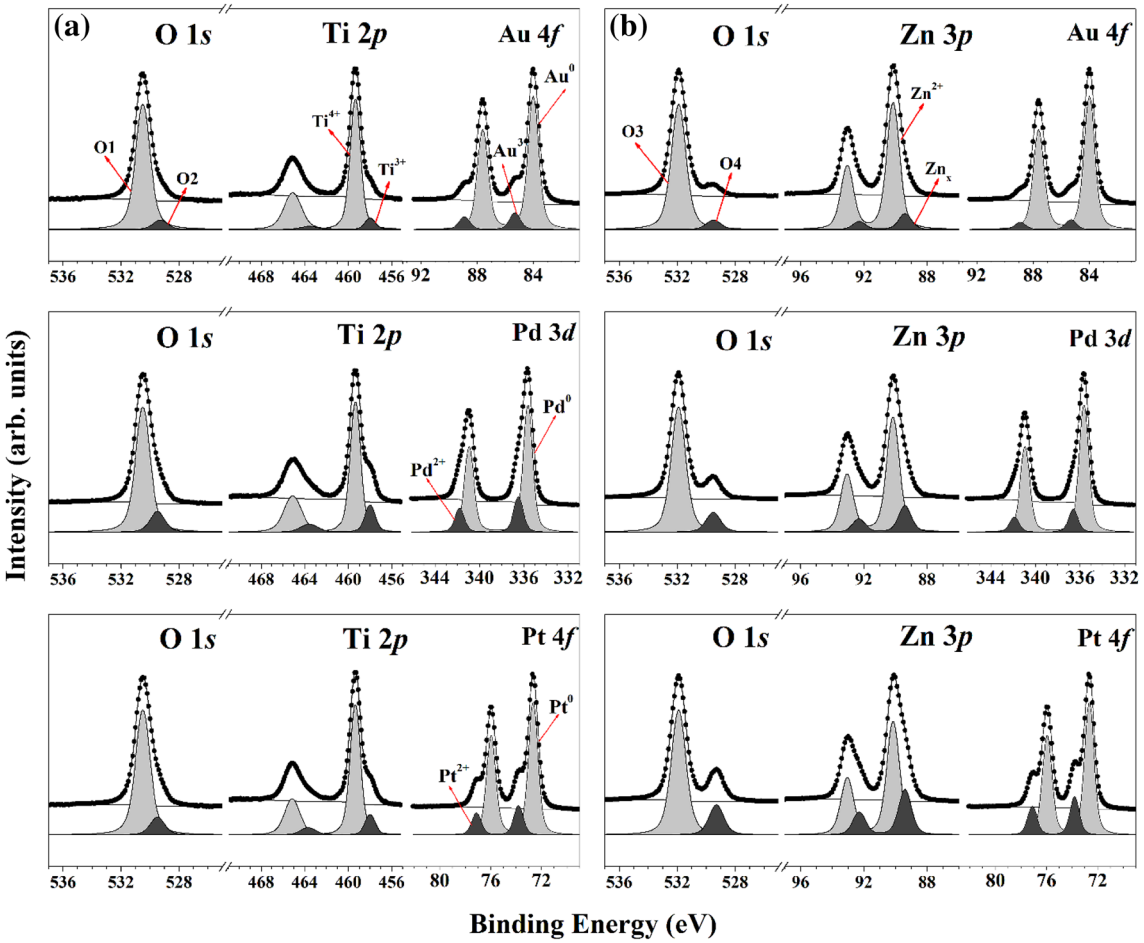

Fig. 1 HRPES results for the 3 wt% noble metals doped in TiO_2 (**a**) and ZnO NPs (**b**). **a** top: O 1*s*, Ti 2*p*, and Au 4*f* of Au-TiO_2, middle: O 1*s*, Ti 2*p*, and Pd 3*d* of Pd-TiO_2, bottom: O 1*s*, Ti 2*p*, and Pt 4*f* of Pt-TiO_2. **b** top: O 1*s*, Zn 3*p*, and Au 4*f* of Au-ZnO, middle: O 1*s*, Zn 3*p*, and Pd 3*d* of Pd-ZnO, bottom: O 1*s*, Zn 3*p*, and Pt 4*f* of Pt-ZnO NPs

A standard test for catalysts of oxidation is the conversion of CO to CO_2. Hence, we monitored the oxidation of CO to CO_2 in the presence of the six samples by using a mass spectrometer for various NP annealing temperatures in the range 300–550 K under UV irradiation. As shown in Fig. 3, we measured the rates of conversion of CO to CO_2 for the six samples at various substrate temperatures (300, 400, 450, and 550 K). Pd-TiO_2, and Pt-ZnO NPs showed higher rates of conversion of CO to CO_2 than did the other NPs, consistent with the EC. Two interesting points emerged from the CO oxidation measurements. First, the concentration of CO_2 produced was dependent on the initial concentration of CO even though the oxygen carriers on the NM-TiO_2 and NM-ZnO NPs can assist CO oxidation. Second, the conversion of CO to CO_2 occurred stably in the range of 300 to 450 K, as shown in Fig. 3. Above 450 K, this conversion rate decreased significantly and did not vary with temperature. And CO oxidation did not occur on any of the six samples above 550 K because the sample annealing temperature was high enough to decompose the molecules (CO and O_2)—that is, the conversion of CO to CO_2 and the decomposition of these molecules may have occurred at the same time. Hence, above 600 K, the conversion rate appeared to be a negative.

Through the analysis, we found that the Pd-TiO_2 and Pt-ZnO NPs showed catalytic activities better than those of the other four systems (Au-TiO_2, Pt-TiO_2, Au-ZnO, and Pd-ZnO NPs). Moreover, for the Pd-TiO_2 NPs, the analysis provided important information about the formation of PdO [27], and indicated that the the Ti–O–Ti bond was weak, which facilitated breaking of the Ti–O bond and resulting in the formation of oxygen vacancies [30–32]. This result revealed the presence of Ti^{3+} cations and the formation of oxygen vacancies, which were related to the subsequent formation of PtO according to Eq. 1.

$$Ti^{4+} - O - Ti^{4+} + Pd \rightarrow Ti^{3+} - \square - Ti^{3+} + PdO. \quad (1)$$

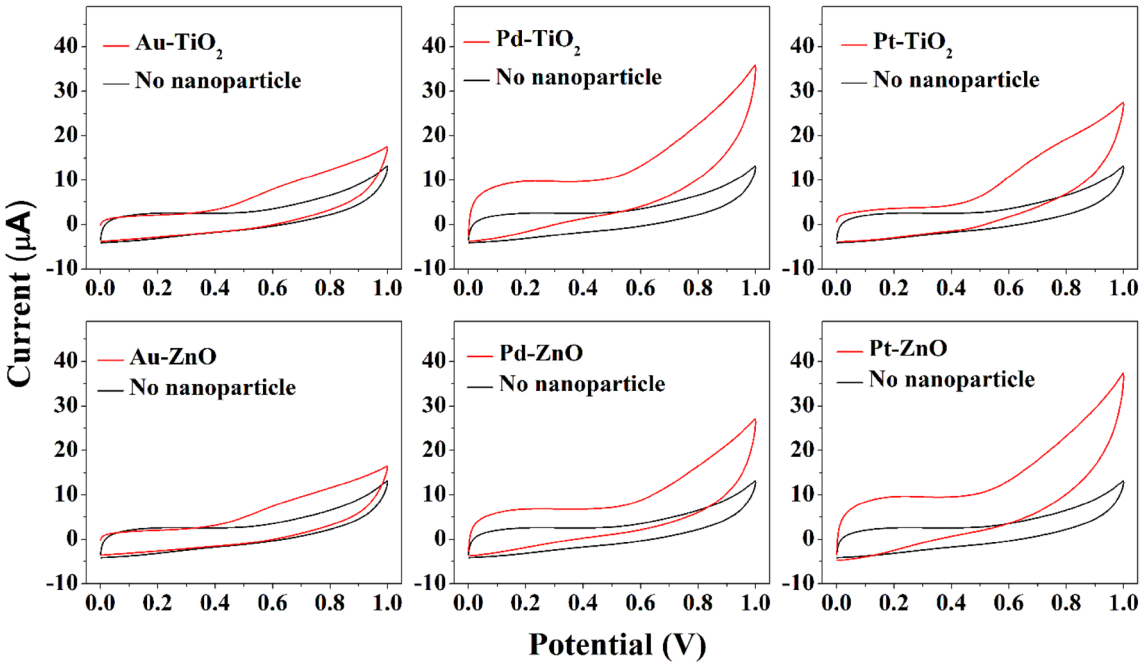

Fig. 2 CVs (at a scan rate of 50 mV/s) of 0.01 M 4-ATP in PBS at bare GCEs (black lines) and at GCEs modified with 3 wt% Au-TiO_2, Pd-TiO_2, Pt-TiO_2, Au-ZnO, Pd-ZnO, and Pt-ZnO (red lines)

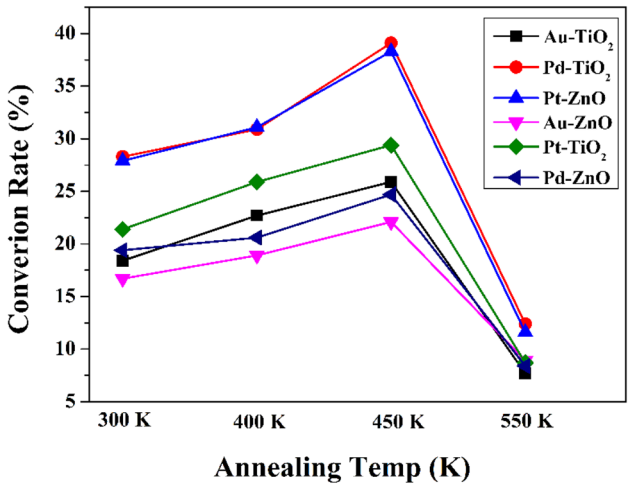

Fig. 3 The variations with substrate temperature in the rates of conversion of CO to CO_2 gas on Au-TiO_2, Pd-TiO_2, Pt-TiO_2, Au-ZnO, Pd-ZnO, and Pt-ZnO NPs

The results for the Pt-ZnO NPs indicated that the formation of Zn^+ defect structures and the corresponding oxygen vacancies followed Eq. 2.

$$Zn^{2+} - O - Zn^{2+} + Pt \rightarrow Zn^{+} - \square - Zn^{+} + PtO. \quad (2)$$

Therefore, we can confidently conclude the Pd-TiO_2 (or Pt-ZnO) NPs to be a critical factor in the formation of Ti^{3+} defects (or Zn^+ defects) and PdO (PtO) particles due to their provide appropriate surfaces for these formations. Many previous studies have demonstrated that defect structures and related oxygen vacancies can contribute to improved photocatalytic activity with metal oxide NPs [33, 34]. The photocatalytic activities of Pd-TiO_2 and Pt-ZnO NPs can be improved by increasing their light absorption, decreasing their photogenerated electron–hole recombination rates, and increasing the rates of their catalytic reactions with charge carriers on their surfaces, and the introduction of defect structures have been reported to increase their activity. That is, surface defects (Ti^{3+} or Zn^+ species) and oxygen vacancies can trap electrons or holes to reduce the electron–hole recombination rate, and holes with prolonged life-times can be utilized to increase the efficiency of the catalytic oxidation reaction. We thus conclude the high catalytic oxidation efficiencies of Pd-TiO_2 and Pt-ZnO NPs to be due to this increased population of defect structures and of PdO (or PtO) on their surfaces.

4 Conclusions

We have demonstrated the formation of PdO and Ti^{3+} (or PtO and Zn^+) on the surfaces of Pd-TiO_2 (or Pt-ZnO) NPs and an enhancement of photo-oxidation reactions on these nanoparticle surfaces as a result of the presence of these species. These surfaces were shown using EC to act as enhanced catalysts to facilitate the oxidation of 4-ATP. As a result, we

confirmed a good positive correlation between the numbers of defect structures induced by the doped noble metals and the catalytic activity, and conclude that, of the six candidate samples, Pd-TiO_2 and Pt-ZnO NPs can act as particularly efficient catalysts due to their relatively large number of defect structures and corresponding oxygen vacancies.

Acknowledgements This research was supported by the National Research Foundation of Korea (NRF) funded by the Korea Government (MSIP) (No. 2017R1A2A2A05001140).

References

1. Qiu Y, Chen W, Yang S (2010) Angew Chem 122:3757–3761
2. Law M, Greene LE, Johnson JC, Saykally R, Yang P (2005) Nature materials 4:455–459
3. Roy P, Kim D, Paramasivam I, Schmuki P (2009) Electrochem Commun 11:1001–1004
4. Ma Y, Wang X, Jia Y, Chen X, Han H, Li C (2014) Chem Rev 114:9987 – 10043
5. Huang MH, Mao S, Feick H, Yan H, Wu Y, Kind H, Weber E, Russo R, Yang P (2001) Science 292:1897–1899
6. Anta JA, Guillén E, Tena-Zaera R (2012) J Phys Chem C 116:11413–11425
7. Waterhouse GIN, Wahab AK, Al-Oufi M, Jovic V, Anjum DH, Sun-Waterhouse D, Llorca J, Idriss H (2013) Sci Rep 3:2849
8. Schaub R, Wahlström E, Rønnau A, Lægsgaard E, Stensgaard I, Besenbacher F (2003) Surf Sci 299:377–379
9. Livraghi S, Paganini MC, Giamello E, Selloni A, Di Valentin C, Pacchioni G (2006) J Am Chem Soc 128:15666–15671
10. Kamarulzaman N, Kasim MF, Rusdi R (2015) Nanoscale Res Lett 10:346
11. Srikant V, Clarke DR (1998) J Appl Phys 83:5447
12. Fang F, Zhao DX, Zhang JY, Shen DZ, Lu YM, Fan XW, Li BH, Wang XH (2007) Nanotechnology 18:235604
13. Hwang Y, Yang S, Lee H (2017) Appl Catal B 204:209–215
14. Al-Azri ZHN, Chen WT, Chan A, Jovic V, Ina T, Idriss H, Waterhouse GIN (2015) J Catal 329:355–367
15. Duh FC, Lee D-S, Chen YW (2013) Mod Res Catal 2:1–8
16. Liu X, Liu M-H, Luo Y-C, Mou C-Y, Lin SD, Cheng H, Chen J-M, Lee J-F, Lin T-S (2012) J Am Chem Soc 134:10251–10258
17. Gogurla N, Sinha AK, Santra S, Manna S, Ray SK (2014) Sci Rep 4:6483
18. Parkinson CR, Walker M, McConville CF (2003) Surf Sci 545:19–33
19. Jung M-C, Kim H-D, Han M, Jo W, Kim D (1999) Jpn J Appl Phys 38:4872
20. Ono LK, Yuan B, Heinrich H, Cuenya BR (2010) J Phys Chem C 114:22119–22133
21. Brun M, Berthet A, Bertolini JC (1999) J Electron Spectrosc Relat Phenom 104:55–60
22. Peuckert M (1985) J Phys Chem 89:2481–2486
23. Kim S, Kim K, Jo Y, Park M, Chae S, Duong DL, Yang CW, Kong J, Lee Y (2011) ACS Nano 5:1236–1242
24. Go Y-J, Yun J-M, Noh Y-J, Yeo J-S, Kim S-S, Jung C-H, Oh S-H, Yang S-Y, Kim D-Y, Na S-I (2013) Appl Phys Lett 102:163302
25. Yang S, Kim Y, Jeon E, Baik J, Kim N, Kim H, Lee H (2016) Catal Commun 81:45–49
26. Hwang Y, Yang S, Jeon E, Lee H (2016) Appl Catal B 180:480–486
27. Lee H, Shin M, Lee M, Hwang Y (2015) Appl Catal B 165:20–26
28. Al-Gaashani R, Radiman S, Daud AR, Tabet N, Al-Douri Y (2013) Ceram Int 39:2283–2292
29. Jeon E, Yang S, Kim Y, Kim N, Shin H, Baik J, Kim H, Lee H (2015) Nanoscale Res Lett 10:361
30. Bharti B, Kumar S, Lee H-N, Kumar R (2016) Sci Rep 6:32355
31. Setvín M, Aschauer U, Scheiber P, Li Y-F, Hou W, Schmid M, Selloni A, Diebold U (2013) Science 341:988–991
32. Cheng H, Selloni A (2009) Phys Rev B 79:092101
33. Janotti A, Van de Walle CG (2005) Appl Phys Lett 87:122102
34. Zhang X, Qin J, Xue Y, Yu P, Zhang B, Wang L, Liu R (2014) Sci Rep 4:4596